

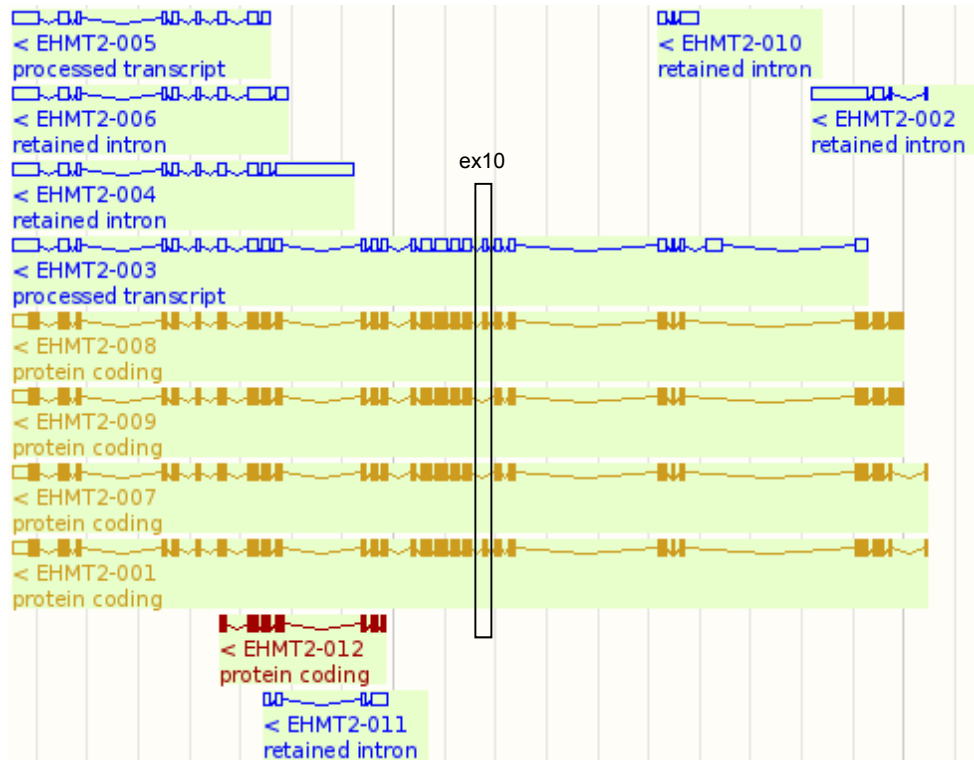
## **SUPPLEMENTARY MATERIAL AND METHODS**

### **Cell culture**

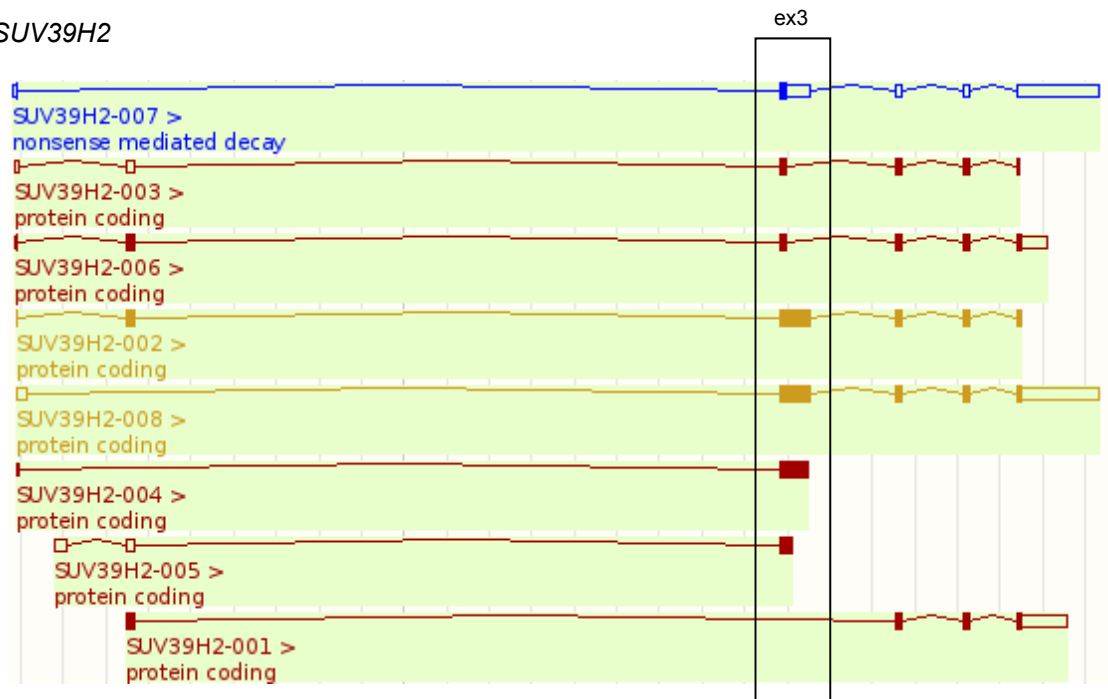
IMR90, Caco-2, HepG2 and SKOV3 (all from ATCC) cells were maintained in Dubelcco's modified Eagle's medium (Gibco, #31966-021) supplemented with 10% (v/v) foetal bovine serum (Thermo Scientific, #SV30160.03) and 100 U/mL penicillin-streptomycin (Gibco, #15140-122). Rhabdoid cells provide by O. Delatre's lab MON (59) were maintained in Roswell Park Memorial Institute medium (Gibco, #61870-010) supplemented with 10% (v/v) foetal bovine serum and 100 U/mL penicillin-streptomycin.

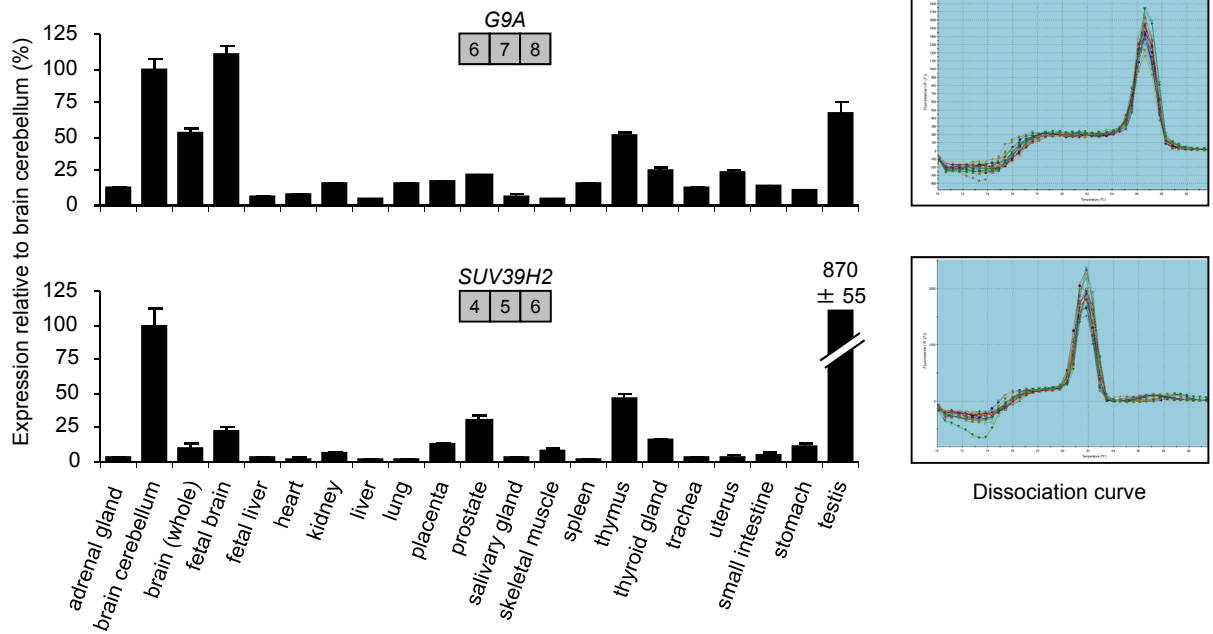
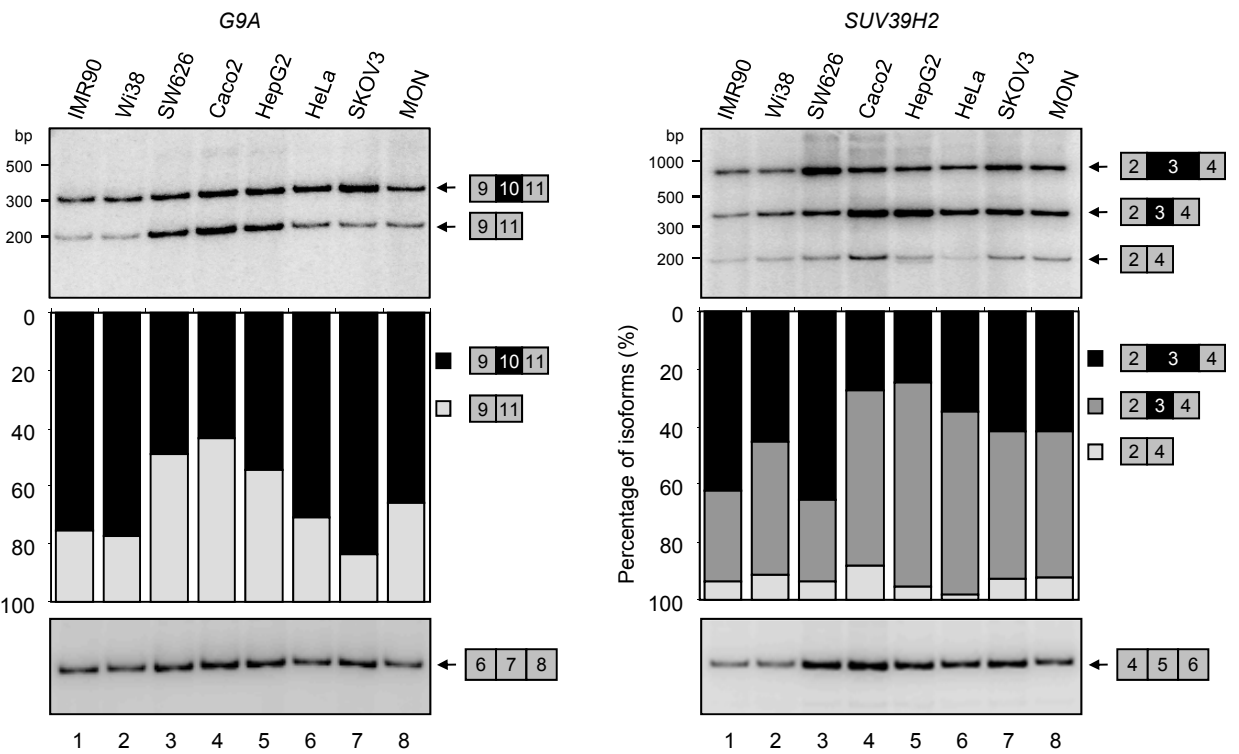
A

G9A

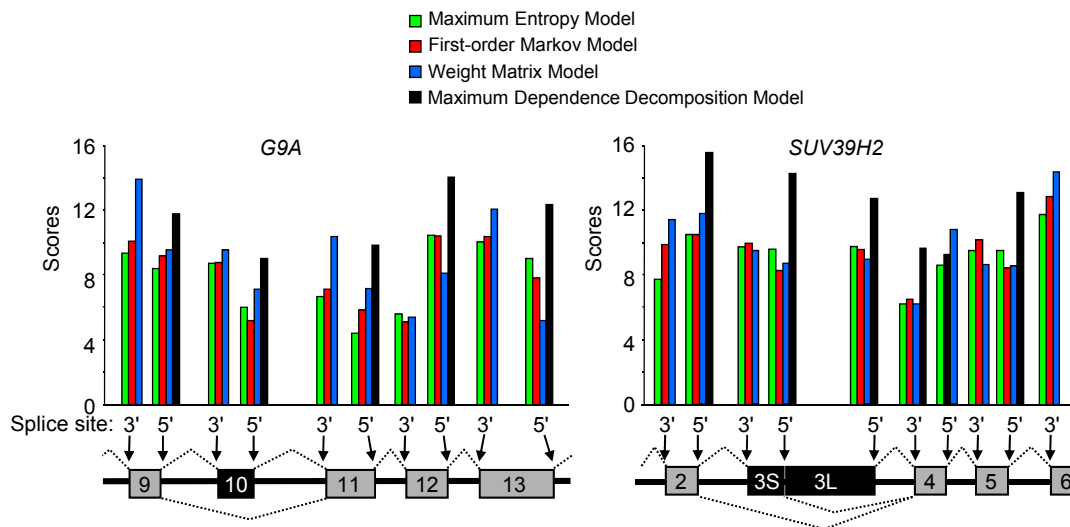


SUV39H2

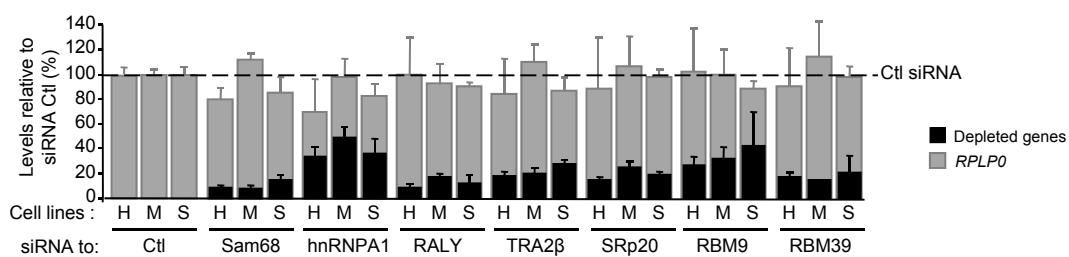


**B****C**

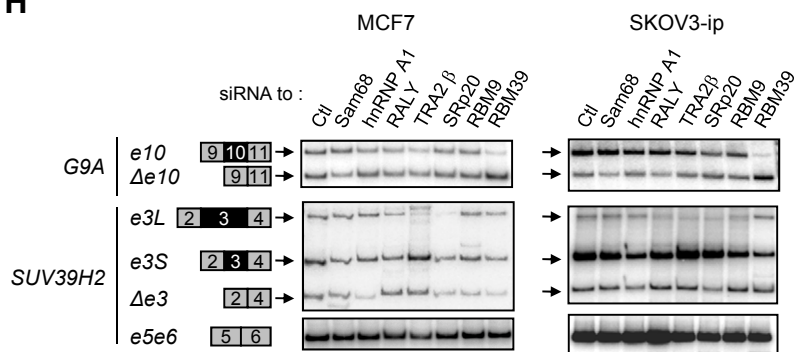
**F**



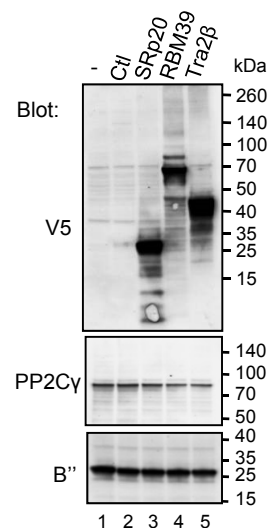
**G**



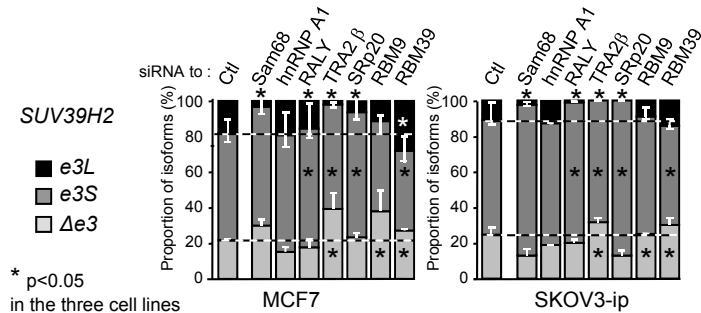
**H**



**J**

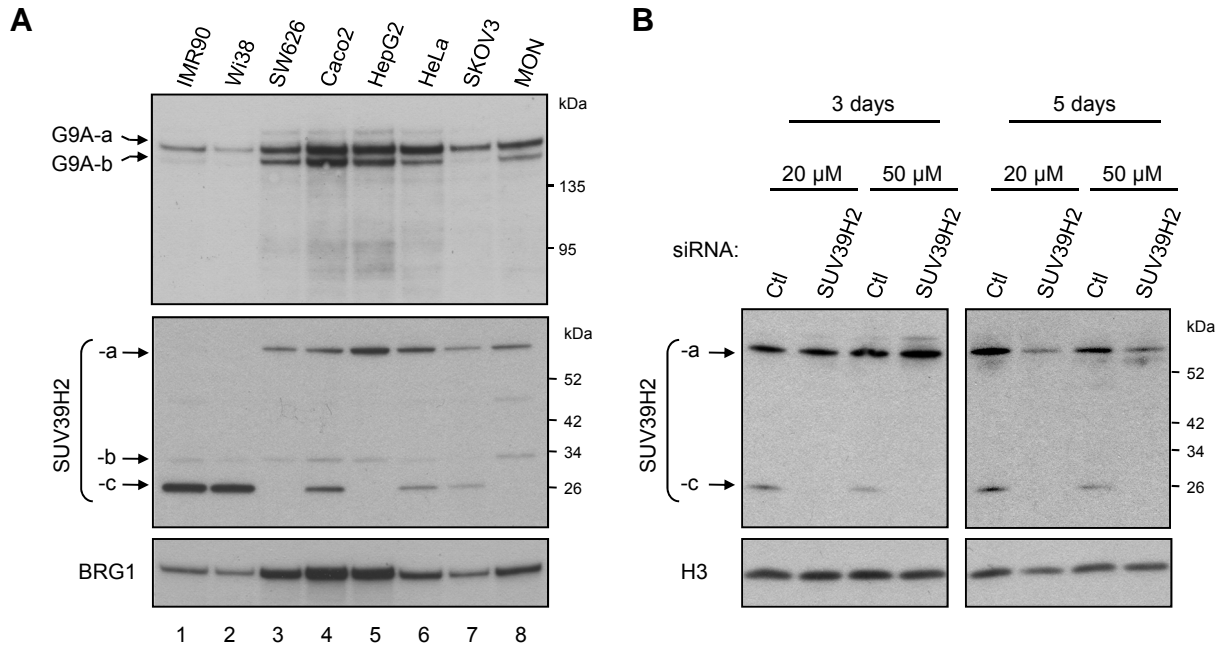


**I**

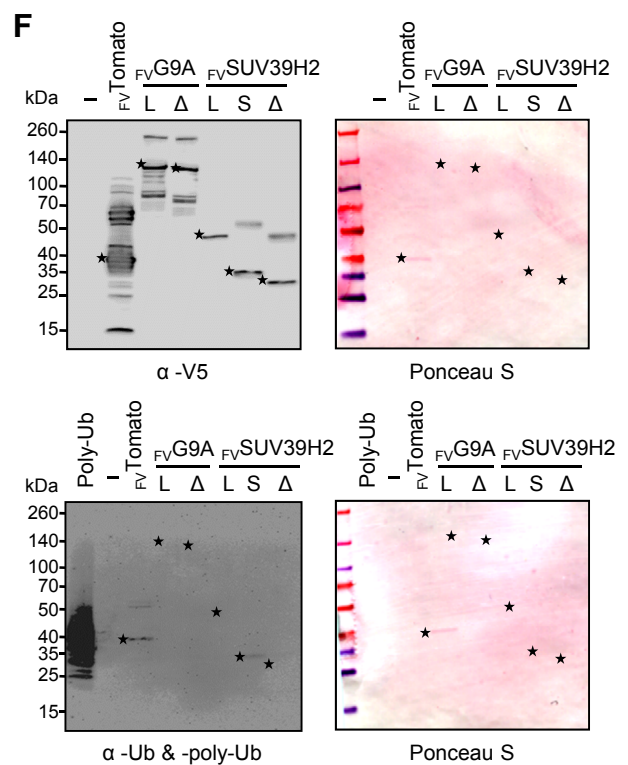
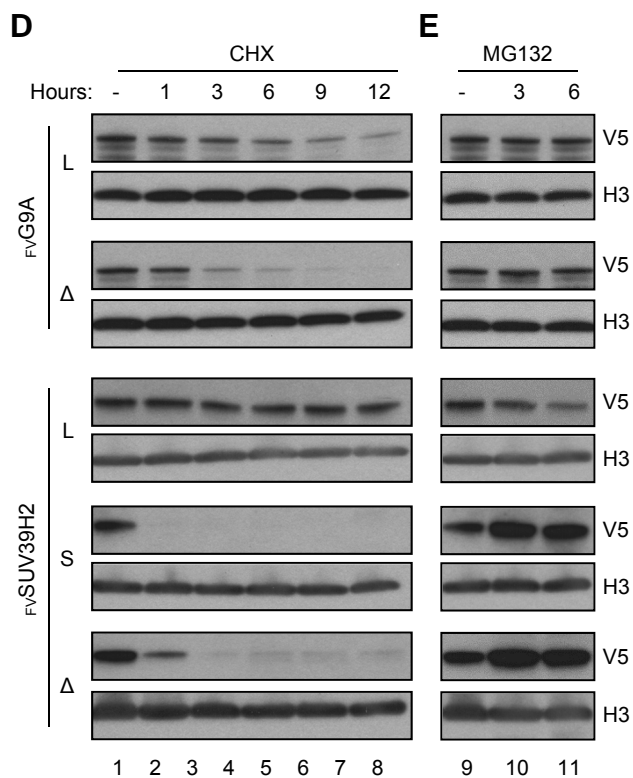
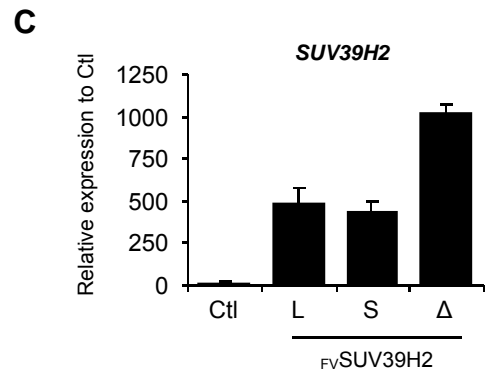
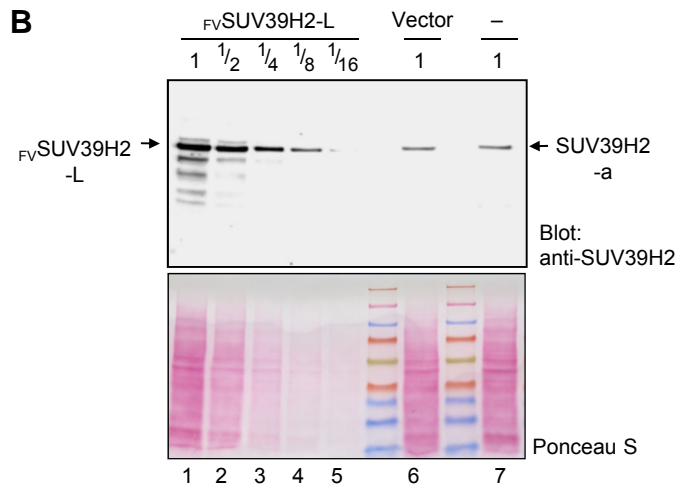
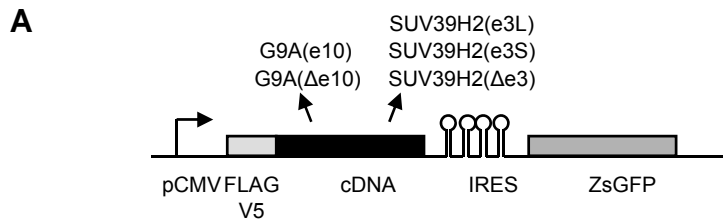


## SUPPLEMENTARY TABLE AND FIGURE LEGENDS

**Supplementary Figure S1 related to Figure 1.** Alternative splicing regulates the expression of *G9A* and *SUV39H2*. **(A)** Screenshot displaying *G9A* (top) and *SUV39H2* (bottom) transcripts annotated in The Ensembl project ([www.ensembl.org](http://www.ensembl.org)). **(B)** Analysis by RT-qPCR of total RNAs from 21 human tissues. The expressions of *G9A* and *SUV39H2* were normalized to cerebellum levels. Dissociation curves of amplicons (right panels) are shown as an evidence of only one PCR product. **(C and D)** Analysis of inclusion of *G9A* exon 10 and *SUV39H2* exon 3 in 8 human cell lines. **(C)** Semi-quantitative RT-PCR was performed with radiolabeled primers and total RNA extracted from the different cell lines (pulmonary fibroblasts IMR90 and WI38, ovarian SW626 and SKOV3, colorectal Caco2, hepatic HepG2, cervical HeLa, and rhabdoid MON cells). **(D)** Quantification of each isoform was displayed using 100% stacked histogram bars. **(E)** Total *G9A* and *SUV39H2* expressions were detected by amplification of constitutive exons. **(F)** *In silico* prediction of 5' and 3' splice site strength of *G9A* and *SUV39H2* exons. Indicated models were used from the Burge's lab web site to estimate the strength of splice sites (76). No evidence of particular weakness of alternative exons is observable; for instance, the strength of 3' splice site of *G9A* exon 12 and *SUV39H2* exon 4 are weaker than those calculated for exon 10 and exon 3S, respectively. **(G)** Analysis by RT-qPCR of siRNA-mediated depletion of splicing factor mRNAs was performed in three cell lines: HeLa (H), MCF7 (M) and SKOV3-ip (S). The RNA level of each splicing factor and *RPLP0* was normalized to non targeting siRNA (Ctl). **(H and I)** Analysis of *G9A* exon 10 and *SUV39H2* exon 3 in MCF7 and SKOV3-ip cells after siRNA-mediated depletion of splicing factors. Levels of PCR products were analyzed as in **Figure 1B** and **1C**. **(J)** Overexpression of splicing factors was revealed by Western blot using anti-V5 antibody. PP2C $\gamma$  and B" proteins were detected as loading controls.

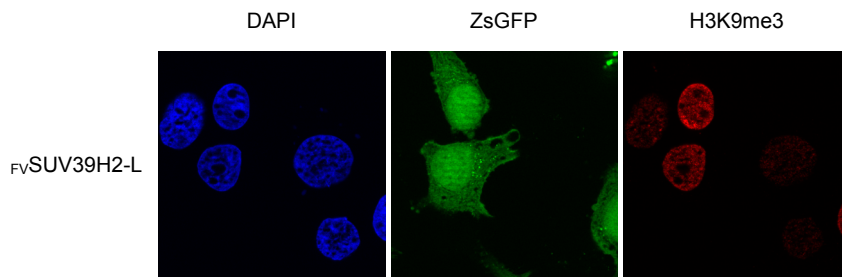
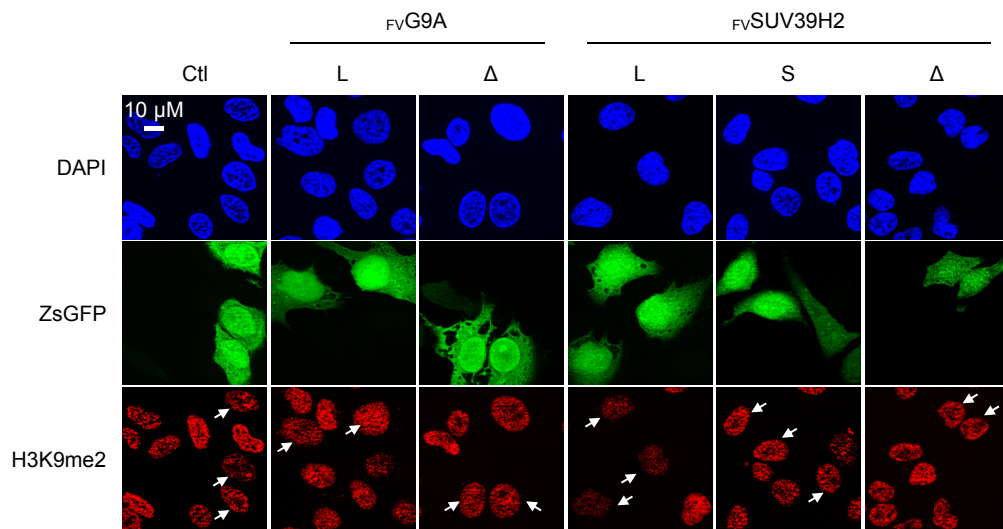
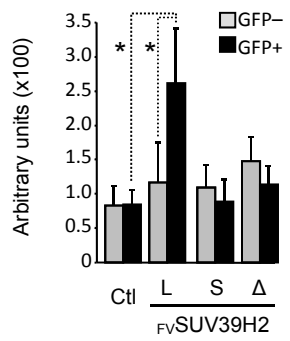


**Supplementary Figure S2 related to Figure 2.** *G9A* and *SUV39H2* produce several protein isoforms. *G9A* and *SUV39H2* protein isoforms were analysed as in Figure 2C in 8 human cell lines (**A**), after a kinetic of siRNA-mediated depletion for 20 or 50  $\mu$ M of siRNA (**B**).

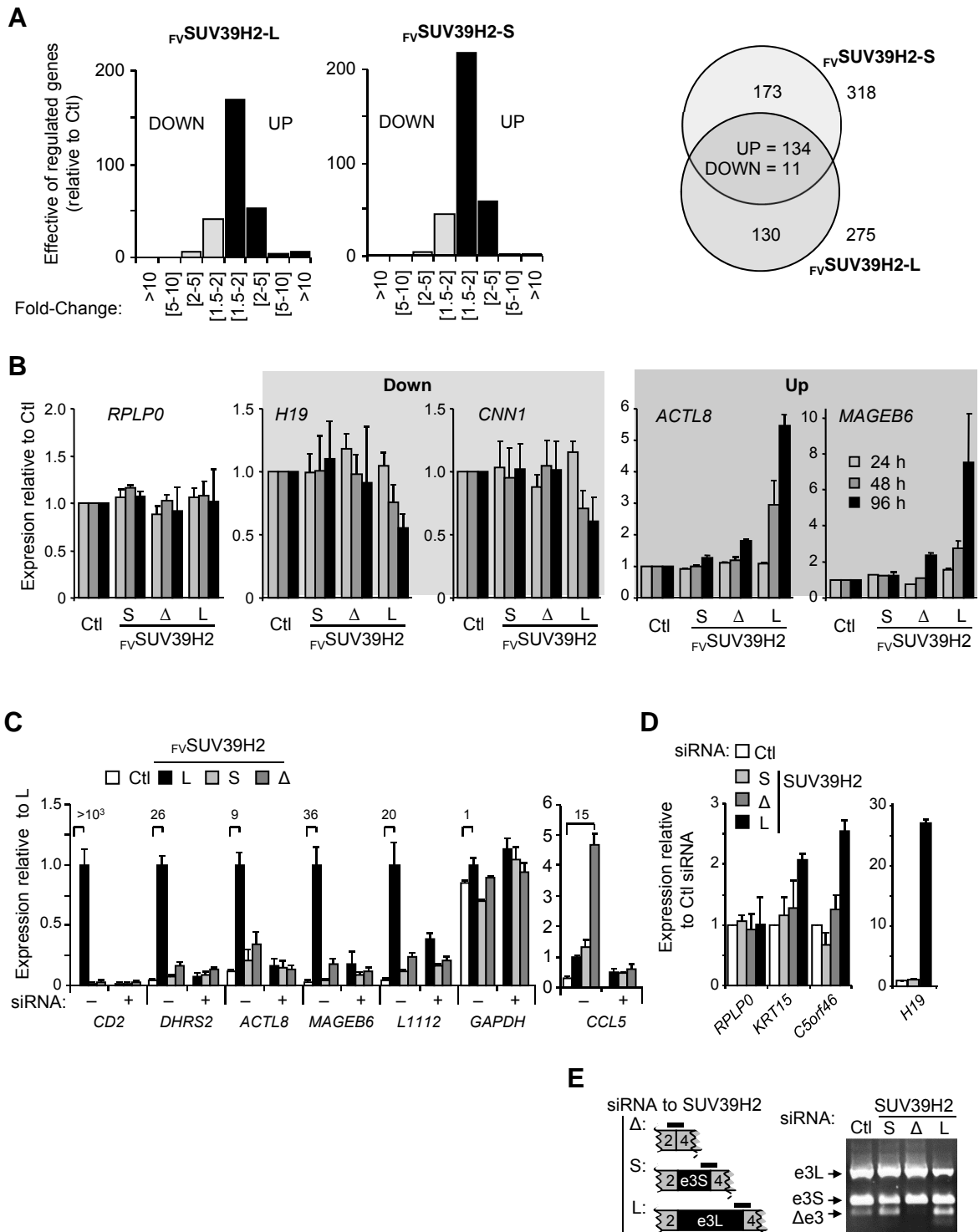


**Supplementary Figure S3 related to Figure 3.** Protein stability of SUV39H2 isoforms are regulated by alternative inclusion of exon 3. **(A)** Scheme displaying the bicistronic construct used to express *FV*G9A or *FV*SUV39H2 cDNA and ZsGreen1 Fluorescence Protein (ZsGFP) under control of CMV promoter (pCMV). **(B)** Overexpression of *FV*SUV39H2-L and endogenous SUV39H2 proteins in HeLa cells were revealed by Western blot using anti-SUV39H2 antibody mixture as indicated in material and methods section. Equal quantity of whole protein extracts prepared from Ctl cells (lane 6), untransduced cells (lane 7) or *FV*SUV39H2-L-expressing cells (lane 1) were compared by assessment of SUV39H2 proteins. The level of over-expression was estimated to 8 fold using serial dilution of *FV*SUV39H2-L-expressing cell extract (lanes 2-5). **(C)** Levels of *SUV39H2* expression detected RT-qPCR in cells expressing *FV*SUV39H2-L, -S, or - $\Delta$  or transduced with control (Ctl). **(D and E)** Analysis of *FV*G9A and *FV*SUV39H2 isoforms was assessed by Western blot in HeLa cells untreated (-, lanes 1 and 9) or treated with cycloheximide (CHX) **(D)** or MG132 **(E)** for the indicated times in hours (h). **(F)** Ubiquitination analysis of G9A and SUV39H2 isoforms. Equal quantity of purified G9A and SUV39H2 proteins (as described in **Figure 4A**) were analysed by Western blot using anti-V5 (top) and P4D1 (bottom) antibodies. Corresponding Ponceau staining of the membranes were shown (right panels). The stars indicate the positions of purified proteins as shown in the V5 blot. Positive control for ubiquitin detection was used by co-analysis of Poly-ubiquitin chains (Ub3-7; K63-linked).



**A****B****C**

**Supplementary Figure S4 related to Figure 4.** Inclusion of *SUV39H2* exon 3 is required to encode an active histone methyltransferase. Immunostaining of H3K9me3 (non saturated picture compared to **Figure 4B**) (**A**) and H3K9me2 (**B**) in HeLa cells expressing  $FV_{G9A}$  and  $FV_{SUV39H2}$  isoforms as in Figure 4.B. (**C**) Quantification of H3K9me3 level detected in immuno-fluorescence assay of **Figure 4B**. Cells over-expressing the  $FV_{SUV39H2}$  isoforms were identified by GFP signal (GFP+) compared to control cells (GFP-). Quantification was assessed with duplicate experiments by quantifying at least sixty nuclei of either GFP positive or negative cells in each condition and the significance of differences was established using Wilcoxon non-parametric test ( $p < 0.01$ ).



**Supplementary Figure S5 related to Figure 5.** Alternative inclusion of SUV39H2 exon 3 modulates the expression of target genes. **(A)** Graph showing the number of genes that are up- or down-regulated in HeLa cells expressing *FV*SUV39H2-L (left panel) or *FV*SUV39H2-S (right panel) as described in Figure 5A. Gene numbers are displayed in function of their fold-change. Number of genes regulated specifically and co-regulated by both isoforms are displayed using a Venn diagram (right panel). **(B)** Transcriptional regulation by SUV39H2 isoforms over time. Two genes down-regulated (Down) and two genes up-regulated (Up) by *FV*SUV39H2-L over-expression were shown relative to control (Ctl). *RPLP0* gene is shown as an unaffected gene. Total RNA extract were performed 1, 2 and 4 days after transduction of exogenous SUV39H2 isoforms. Transcriptional levels of genes were analyzed by RT-qPCR and quantification are displayed as means  $\pm$  s.e.m. of three experimental replicate. **(C)** Validation by RT-qPCR of 6 hits differentially regulated by SUV39H2 isoforms. The significance of this validation was assessed comparing results obtained in HeLa cells transfected (+) or not (-) by siRNA targeting all transcripts of *SUV39H2*. *GAPDH* gene is shown as unaffected gene. **(D)** Release of repressive effect associated to SUV39H2 using isoform-specific depletion of endogenous transcripts. *RPLP0* gene is shown as unaffected gene. **(E)** RNA analysis of SUV39H2 isoform-specific depletion. Target sequences of isoforms-specific siRNAs were symbolised by black bars under alternatively spliced junctions. SUV39H2 isoforms were amplified by RT-PCR and analysed in agarose gel stained with ethidium bromide. Splicing patterns displayed a representative example of three experiments.



Chromatin regulator (alter. name)	Functions of the main product	isoforms	Functions of the alternative splicing isoforms	Refs
DNMT1	DNA methylation	4 isoforms DNMT1o/s/p specific to oocyte, somatic or spermatocyte DNMT1b (exon4)	Localization, translational regulation, sex-specific expression  exon4 : similar kinetic parameters on DNA methylation	(60, 61)
DNMT3B	DNA methylation	40 isoforms DNMT3B4 B5 lacking exons21+22 DNMT3B3-like splice variant lacking exon 5	Exons21+22 encoding catalytic domain  Exon5 increases DNA binding or influences the 3D structure of the adjacent PWWP domain	(62–64)
CARM1 (PRMT4)	Arginine methylase  H3R8	4 isoforms in human, mouse & rat  2 isoforms in <i>X leavis</i>	CARM1-exon v3 regulates alternative splicing of CD44 and E1a  Exon15 encode an automethylated domain of the protein	(65–67)
SIRT1	NAD-dependent deacetylase  H4-K16 and H3-K9 deacetylation	SIRT1-ΔExon8  SIRT1-Δexon2-9	SIRT1- Δ Exon8, displays significant differences in stress-sensitivity, RNA/protein stability, protein-protein interactions and deacetylase activity -Δexon2-9 lacks catalytic domain	(68–70)
PKM1/2	Pyruvate kinase (Warburg effect)	2 isoforms : PKM1 and PKM2	PKM2 phosphorylates H3T11p	(71)
LSD1	H3K4 demethylase	4 isoforms	4 amino acid exon E8a brings the phosphorylated Threonin important for protein conformation and activity	(72, 73)
NURF301	Subunit of chromatin remodeling complex	3 isoforms	Truncated C-terminal isoforms lack ability to target H3K4me3 and H4K16Ac	(74)
EZH2	HMTase of H3K27	2 isoforms EZH2α EZH2β brings Exon4 skipping and Exon8 3'SS	EZH2β represses a predominantly unique subset of gene targets from EZH2α	(75)

**Supplementary Table S1:** Few examples of chromatin regulators functionally studied in toward their alternative spliced isoforms







Sample	Raw reads	Average base quality over 30	Sequence length	%GC	Total mapped reads
pLVX_1	57,683,411	100%	50	51	(93.5%) 53,336,056
pLVX_2	55,270,068	100%	50	50	(96.1%) 52,723,331
pLVX_3	42,509,141	100%	50	50	(96.2%) 40,592,080
G9a_e10_1	39,316,485	100%	50	51	(93.0%) 36,084,509
G9a_e10_2	56,272,391	100%	50	50	(96.4%) 53,851,594
G9a_e10_3	29,995,057	100%	50	50	(96.6%) 28,768,149
G9a_Δe10_1	30,951,069	100%	50	51	(96.8%) 29,729,406
G9a_Δe10_2	44,665,122	100%	50	50	(96.7%) 42,872,820
G9a_Δe10_3	47,980,571	100%	50	50	(96.9%) 46,160,588
SUV39H2_e3L_1	35,387,857	100%	50	50	(96.2%) 33,809,030
SUV39H2_e3L_2	36,529,662	100%	50	50	(96.0%) 34,815,356
SUV39H2_e3L_3	65,932,495	100%	50	50	(96.0%) 62,871,033
SUV39H2_e3S_1	26,309,193	100%	50	50	(96.2%) 25,122,569
SUV39H2_e3S_2	49,701,123	100%	50	51	(96.2%) 47,465,352
SUV39H2_e3S_3	53,407,232	100%	50	50	(96.2%) 51,009,422

**Supplementary Table S4 : RNA-Seq statistics**

## SUPPLEMENTARY REFERENCES

59. Medjkane,S., Novikov,E., Versteeg,I. and Delattre,O. (2004) The tumor suppressor hSNF5/INI1 modulates cell growth and actin cytoskeleton organization. *Cancer Res.*, 64, 3406–3413.
60. Mertineit,C., Yoder,J.A., Taketo,T., Laird,D.W., Trasler,J.M. and Bestor,T.H. (1998) Sex-specific exons control DNA methyltransferase in mammalian germ cells. *Development*, 125, 889–897.
61. Bonfils,C., Beaulieu,N., Chan,E., Cotton-Montpetit,J. and MacLeod,A.R. (2000) Characterization of the Human DNA Methyltransferase Splice Variant Dnmt1b. *J. Biol. Chem.*, 275, 10754–10760.
62. Robertson,K.D., Uzvolgyi,E., Liang,G., Talmadge,C., Sumegi,J., Gonzales,F.A. and Jones,P.A. (1999) The human DNA methyltransferases (DNMTs) 1, 3a and 3b: coordinate mRNA expression in normal tissues and overexpression in tumors. *Nucleic Acids Res.*, 27, 2291–2298.
63. Gopalakrishnan,S., Emburgh,B.O.V., Shan,J., Su,Z., Fields,C.R., Vieweg,J., Hamazaki,T., Schwartz,P.H., Terada,N. and Robertson,K.D. (2009) A Novel DNMT3B Splice Variant Expressed in Tumor and Pluripotent Cells Modulates Genomic DNA Methylation Patterns and Displays Altered DNA Binding. *Mol. Cancer Res.*, 7, 1622–1634.
64. Van Emburgh,B.O. and Robertson,K.D. (2011) Modulation of Dnmt3b function in vitro by interactions with Dnmt3L, Dnmt3a and Dnmt3b splice variants. *Nucleic Acids Res.*, 39, 4984–5002.
65. Matsuda,H., Paul,B.D., Choi,C.Y. and Shi,Y.-B. (2007) Contrasting Effects of Two Alternative Splicing Forms of Coactivator-Associated Arginine Methyltransferase 1 on Thyroid Hormone Receptor-Mediated Transcription in *Xenopus laevis*. *Mol. Endocrinol.*, 21, 1082–1094.
66. Ohkura,N., Takahashi,M., Yaguchi,H., Nagamura,Y. and Tsukada,T. (2005) Coactivator-associated Arginine Methyltransferase 1, CARM1, Affects Pre-mRNA Splicing in an Isoform-specific Manner. *J. Biol. Chem.*, 280, 28927–28935.
67. Wang,L., Charoensuksai,P., Watson,N.J., Wang,X., Zhao,Z., Coriano,C.G., Kerr,L.R. and Xu,W. (2013) CARM1 automethylation is controlled at the level of alternative splicing. *Nucleic Acids Res.*, 41, 6870–6880.
68. Pruitt,K., Zinn,R.L., Ohm,J.E., McGarvey,K.M., Kang,S.-H.L., Watkins,D.N., Herman,J.G. and Baylin,S.B. (2006) Inhibition of SIRT1 reactivates silenced cancer genes without loss of promoter DNA hypermethylation. *PLoS Genet.*, 2, e40.
69. Lynch,C.J., Shah,Z.H., Allison,S.J., Ahmed,S.U., Ford,J., Warnock,L.J., Li,H., Serrano,M. and Milner,J. (2010) SIRT1 Undergoes Alternative Splicing in a Novel Auto-Regulatory Loop with p53. *PLoS ONE*, 5, e13502.
70. Shah,Z.H., Ahmed,S.U., Ford,J.R., Allison,S.J., Knight,J.R.P. and Milner,J. (2012) A Deacetylase-Deficient SIRT1 Variant Opposes Full-Length SIRT1 in Regulating Tumor Suppressor p53 and Governs Expression of Cancer-Related Genes. *Mol. Cell. Biol.*, 32, 704–716.
71. Yang,W., Xia,Y., Hawke,D., Li,X., Liang,J., Xing,D., Aldape,K., Hunter,T., Alfred Yung,W.K. and Lu,Z. (2012) PKM2 Phosphorylates Histone H3 and Promotes Gene Transcription and Tumorigenesis. *Cell*, 150, 685–696.
72. Zibetti,C., Adamo,A., Binda,C., Forneris,F., Toffolo,E., Verpelli,C., Ginelli,E., Mattevi,A., Sala,C. and Battaglioli,E. (2010) Alternative Splicing of the Histone Demethylase LSD1/KDM1 Contributes to the Modulation of Neurite Morphogenesis in the Mammalian Nervous System. *J. Neurosci.*, 30, 2521–2532.
73. Toffolo,E., Rusconi,F., Paganini,L., Tortorici,M., Pilotto,S., Heise,C., Verpelli,C., Tedeschi,G., Maffioli,E., Sala,C., et al. (2013) Phosphorylation of neuronal Lysine-Specific

- Demethylase 1LSD1/KDM1A impairs transcriptional repression by regulating interaction with CoREST and histone deacetylases HDAC1/2. *J. Neurochem.*, 10.1111/jnc.12457.
74. Kwon,S.Y., Xiao,H., Wu,C. and Badenhorst,P. (2009) Alternative splicing of NURF301 generates distinct NURF chromatin remodeling complexes with altered modified histone binding specificities. *PLoS Genet.*, 5, e1000574.
75. Grzenda,A., Lomberk,G., Svingen,P., Mathison,A., Calvo,E., Iovanna,J., Xiong,Y., Faubion,W. and Urrutia,R. (2013) Functional characterization of EZH2beta reveals the increased complexity of EZH2 isoforms involved in the regulation of mammalian gene expression. *Epigenetics Chromatin*, 6, 3.
76. Yeo,G. and Burge,C.B. (2004) Maximum entropy modeling of short sequence motifs with applications to RNA splicing signals. *J. Comput. Biol. J. Comput. Mol. Cell Biol.*, 11, 377–394.